Journal of Alloys and Compounds xxx (xxxx) xxx

Contents lists available at ScienceDirect

Journal of Alloys and Compounds

journal homepage: http://www.elsevier.com/locate/jalcom

Waste rice husk ash derived sol: A potential binder in high alumina refractory castables as a replacement of hydraulic binder

SK. S. Hossain, P.K. Roy*

Department of Ceramic Engineering, IIT (BHU), Varanasi, 221005, UP, India

ARTICLE INFO

Article history:
Received 29 April 2019
Received in revised form
26 September 2019
Accepted 25 October 2019
Available online xxx

Keywords:
Sol binder
Nano silica
Rice husk ash
Castable
Physico-mechanical
Slag corrosion

ABSTRACT

This work provides a new source of binder system, i.e., waste rice husk ash (RHA) derived sol for unshaped refractories. A facile (alkali extraction) route is used to synthesize the sol from the waste RHA. The sol consists of single phase amorphous silica with average particle size around 22 nm. The estimated cost of 30 wt% solid containing RHA derived sol per litre is around 9.35 $. The temperature of mullite ($3Al_2O_3 \cdot 2SiO_2$) formation from waste derived sol and reactive alumina containing system is 1250 °C or higher. The sol (30 wt% SiO_2) and the dry sol (99.32 wt% SiO_2) is used to formulate the high alumina castable samples. The sintering is performed at 1400 °C, 1500 °C and 1550 °C. The different physico-mechanical characterizations and blast furnace slag (BFS) corrosion test at 1500 °C are comprehensively investigated with the prepared castables. The properties of 5 wt% silica (3 wt% from sol and 2 wt% dry sol) containing castable specimens are also equated with the commercially available different silica containing high alumina castable systems. The obtain results are good agreements with the source data. These promising characteristic confirms the possibility of using waste RHA derived sol for manufacturing of cement free high alumina castable and leads to the economic and ecological benefits in the refractory industries.

1. Introduction

The refractory castable contains generally two different constituents, i.e., major part is non-continuous refractory grade aggregates and another part is continuous matrix or bonding phase. The interactions between these two constituents are regulating the final properties of the castables. Therefore, the selection of the bonding or matrix phase, which is greatly affecting the product characteristics, is highly sensitive for making the refractory castable. The binder phase delivers both strengths at green body and at higher temperature by forming high temperature phases or by enhancing the sintering kinetics through the decomposition on heating [1,2].

Generally, used binder in refractory castable is calcium aluminate cement (CAC). However, it has some limitations, like formation of low melting eutectic phases through the reaction of CaO with SiO_2 and Al_2O_3, for high temperature (>1500 °C) applications. It degrades the corrosion resistance and the high temperature mechanical strength of the castable [3,4]. So, the focuses of the researchers have now been shifted to the no cement bonding or matrix systems for high temperature applications [4–7]. Recently, colloidal silica, sol-gel derived sol or silica fume and other micro fine or nano silica sources have been played an important role as an alternative of CAC in the castable [4,7–9]. The addition of silica sol in the refractory castables has some advantages like less or no water requirement, short mixing time, high drying rate, high permeability, low spalling risk and introduced sustainable green strength by gelation mechanism [10,11]. Furthermore, the nano-size reactive silica containing sol may endorse the formation of mullite ($3Al_2O_3 \cdot 2SiO_2$) in alumina containing refractory castables after firing [1,8,9]. The presence of mullite matrix phase in the castable helps to improve the various properties such as high temperature stability, chemical stability, low thermal expansion, high refractoriness, good strength and toughness of the refractory [12]. Therefore, colloidal or silica fume is commercially exploited as an alternative refractory binding system and it is expected to increase the demands in the near future. Consequently, the preparation of these nano-size precursors is difficult and expensive. It affects the cost of the final products. To develop a facile, sustainable and economical route for the preparation of nano silica containing

* Corresponding author.
E-mail addresses: skshossain.rs.cer17@iitbhu.ac.in (SK.S. Hossain), pkroy.cer@iitbhu.ac.in (P.K. Roy).

https://doi.org/10.1016/j.jallcom.2019.152806
0925-8388/

sources is challenging for the researchers. Lim et al. [13] have described the several synthesis methods, i.e., hydrolysis and condensation of silicate compound, direct oxidation of silicon, and ion exchange of sodium silicate, for the preparation of colloidal silica. Hyde et al. [14] have provided an overview about the up-to-date laboratory and industrial-based colloidal, fume and nano silica synthesis routes. Each of the process retains its own advantages and limitations according to the commercialization and tailor properties of the product. Rice husk (RH) or waste rice husk ash (RHA) derived silica sol or nano silica can also be used as an alternative silica source for refractory castables.

RH is an outer cover of paddy grain and it is about 20–30 wt% of harvested paddy rice. It is produced through the milling process of rice [15]. Recently, RH is generally used as a fuel in the boilers due to generate significant heat (13–16 MJ/kg) during the combustion [16]. After burning of RH, it is produced a waste, i.e., rice husk ash (RHA), which is 18–25% of initial weight of RH. This waste has no larger application areas rather than land-filling. Therefore, RHA is abundantly available outside the rice mill and it is created environmental pollution along with disposal problem [17]. However, RHA retains around 80–95 wt% of amorphous silica, which has huge industrial importance as a replacement of conventional silica sources [18–20]. Due to an increasingly wide market of amorphous silica, researchers are engaged to find out the economical routes to extract nano silica from RHA. Alkali extraction is an inexpensive method, which is able to prepare high purity silica sol or nano silica powder for different mullite based ceramics [21–23]. Sembiring et al. [24] have prepared mullite ceramic from RHA derived silica. Serra et al. [25] have revealed a reaction-sintering technique for the formation of mullite from RHA. Fernandes and Salomão [26] have disclosed that the RHA or RH derived silica with calcined alumina has formed in-situ mullite formation. To the best of our knowledge, no such investigation has been found, where, waste RHA derived sol is used as a binder and in-situ mullite formation with derived sol in high alumina refractory castable.

The present study is explored a novel approach to investigate the feasibility of using RHA derived silica sol as a binder system for high alumina refractory castable. Alkali extraction method is adopted for the synthesis of silica sol from RHA. Additionally, mullite formation ability of this waste derived sol with reactive alumina is systematically investigated. Highlighting is given to the in-situ mullite formation and the physico-mechanical properties of the synthesized castables. The corrosion behavior with the blast furnace slag (BFS) at 1500 °C is also discussed. The obtained properties of the in-situ mullite matrix containing castable are compared with the commercially available different silica containing high alumina refractory castable systems.

2. Experimental

2.1. Materials

The waste RHA was collected from local rice mill ("Samrat rice mill", Burdwan, India), where, RH was used as a fuel in the boiler. The physico-chemical analysis of RHA was previously reported [27]. It retained above ~93 wt% of amorphous silica [27]. Analytical grade (AR) hydrochloric acid (assay 35%), sodium hydroxide plates (assay 99%), reactive alumina (assay 99%) and calcined alumina (assay 99%) were bought from Loba Chemie Pvt. Ltd., India. The CAC (CA-25 M) and brown tabular alumina (98.16% Al_2O_3) were purchased from Almatis, India and S. D. Fine Chem. Ltd., India, respectively. The distilled water was used for all the synthesis process.

2.2. Silica sol synthesis

Fig. 1 depicts the preparation flow chart of waste RHA derived silica sol, mullite formation and high alumina castable. Silica sol was obtained from waste RHA using alkali extraction route, which was deeply discussed in our previous work [28]. 90 μm sieving RHA was first cleaned at room temperature with 0.5 N HCl solutions under continuous magnetic stirring for 30 min to remove any possible present metal impurities or dirt's. 0.75 wt ratios of clean RHA and NaOH pallet was mixed with the distilled water (1 lt. water with 100 g mixture) in a glass beaker at 90 °C for 1 h. For accomplishment of the reaction (reaction 1), the mixture solution was rested for 24 h at ambient temperature. The unreacted solid part was separated from sodium silicate solution through millipore filter papers. The filtrated silicate solution was slowly acidified by the addition of HCl under constant stirring until the transparent solution was completely precipitated into a white silica gel (reaction 2). The gel was left for aging for 1 day, and then repetitively washed through the deionized water to eliminate the Na^+ or other ions. The acquired product was then controlled by the heat treated at 80 °C to remove excess free water. The following chemical reaction can be represented for the formation of silica sol from RHA [28]:

$$SiO_2(RHA) + 2NaOH \rightarrow Na_2SiO_3 + H_2O \quad (1)$$

$$Na_2SiO_3 + HCl \rightarrow SiO_2(gel) + NaCl\ (sol.) + H_2O \quad (2)$$

2.3. Mullite synthesis

RHA derived silica sol and reactive alumina was mixed to know the mullite phase ($3Al_2O_3{\cdot}2SiO_2$) formation temperature. Therefore, stoichiometric (3:2) amount of reactive alumina and silica (30 wt% solid containing sol) was mixed in a high energy ball mill with 600 rpm for 1 h. Later, the mix mass was dried at 110 °C. For pelletization, the powder was pressed by a uniaxial hydraulic press with 50 MPa pressure. The green pellets were heat-treated at 1100, 1200, 1250 °C for 2 h in an air atmosphere.

2.4. Castable making

Five different castable compositions were prepared by mixing of brown tabular alumina as aggregates (different sizes), calcined alumina, reactive alumina, CAC, silica sol and very less amount of sodium hexametaphosphate (SHMP), as a dispersant agent. The composition of the different samples and the size distribution of the ingredients are depicted in Table 1 s-0 composition was prepared by CAC binding system. Whereas, s-1 composition was fabricated by partially replacing of CAC through the silica sol. s-2 samples onwards compositions were made by the addition of silica sol and dry silica sol (to avoid excessive water in the castable) in the place of CAC. Last two (s-3 and s-4) compositions were prepared by the addition of dry silica sol in place of calcined alumina. Initially, SHMP, reactive alumina, calcined alumina and both silica sol or CAC were mixed for 10 min and then aggregates, i.e., different fraction (for good packing efficiency of castable) of brown tabular alumina were added and mixed for another 5 min. Different shapes of castable specimens were prepared by the pouring of mixed mass into different sizes ($25 \times 25 \times 10\ mm^3$ and $50 \times 10 \times 10\ mm^3$ rectangular, $25\ mm^3$ cube) properly oiled steel moulds. For better compactness, the mix filled moulds were casted by the vibro-caster for 5 min. The cement containing (s-0 and s-1) samples were released from the moulds after 2 h of casting for development of

Please cite this article as: S.S. Hossain, P.K. Roy, Waste rice husk ash derived sol: A potential binder in high alumina refractory castables as a replacement of hydraulic binder, Journal of Alloys and Compounds, https://doi.org/10.1016/j.jallcom.2019.152806

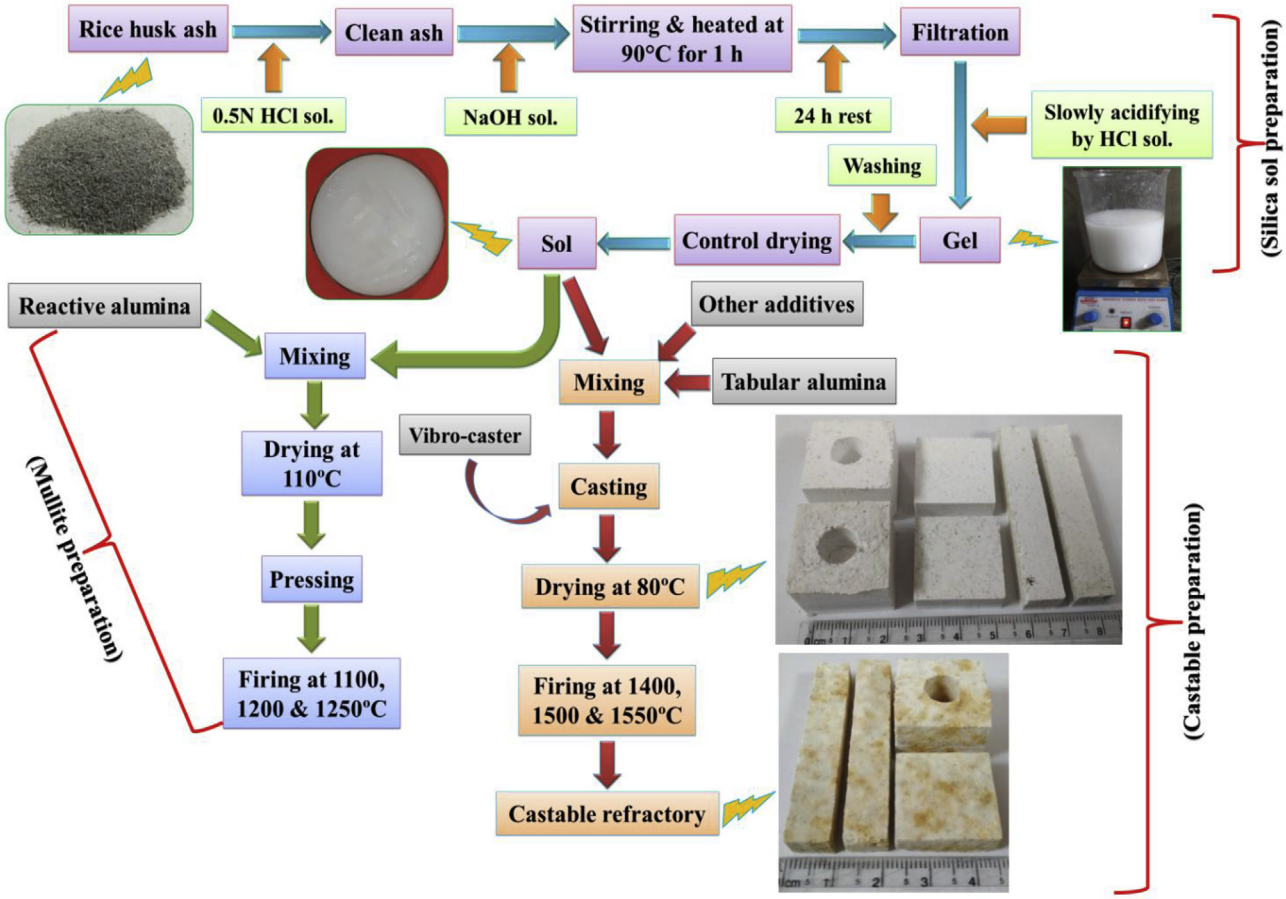

Fig. 1. Preparation scheme of RHA derived sol, mullite formation and high alumina refractory castable.

Table 1
Sample's nomenclature and composition.

Samples	Tabular alumina (wt.%)			Calcined alumina (wt.%), (<2 μm)	Reactive alumina (wt.%), (<1 μm)	CAC (wt.%), (<9 μm)	Silica sol (present SiO_2, wt.%)	Dry sol (wt.%)	SHMP (wt.%)	Water (wt.%)
	(1 −3 mm)	(0.1 −1 mm)	(<0.1 mm)							
s-0	30	20	20	9.8	16	4	0	0	0.2	5
s-1	30	20	20	9.8	16	2	2	0	0.2	2
s-2	30	20	20	9.8	16	0	3	1	0.2	0
s-3	30	20	20	8.8	16	0	3	2	0.2	0
s-4	30	20	20	7.8	16	0	3	3	0.2	0

workable hardening and then the samples were cured in a ~80% relative humidity containing humidity chamber for about 24 h at room temperature to complete hydration reactions. On the other hand, sol containing castable samples (s-2, s-3 and s-4) was carefully released from the moulds after 15 min of casting. It didn't require any separate curing stages due to sustainable strength was developed before drying process through the coagulation (the water from the sol was started to absorb by the other dry aggregates during casting process and helped to decrease the inter-particle separation distance of sol nano particles with increasing the particle collision) of sol containing nano particles [10]. Later, the all casted specimens were very carefully transferred into an air dryer to dry at 80 °C for 12 h. Sintering was performed in a muffle furnace at 1400, 1500 and 1550 °C for 4 h with a heating and cooling rate of 2 °C/min to yield the castable refractories.

2.5. Characterizations

The solid content of RHA derived sol was evaluated by the heating of sol up to 1200 °C in an air atmosphere. The chemical composition present of this solid was analyzed by the X-ray fluorescence (XRF) (Philips PW 2400, Netherlands). The pH value of the sol was measured by the digital pH meter (Toshcon Industries Pvt. Ltd., Ajmer, India). The shape and size of present particles in the sol was determined by the transmission electron microscopy (TEM) (FEI, TECNAI G2-20 TWIN, Netherlands). Differential thermal and thermogravimetric (DTA-TGA) measurement for mullite formulation was done up to 1300 °C with a heating rate of 10 °C/min in an air atmosphere (Model- Labsys KEP- Technologies, Serial no-560/51920, Setaram-Scientific & Industrial Equipment, France). The formation of mullite and phase formation in the sintered castables was identified by X-ray diffraction (XRD) analysis with X'Pert Pro

Please cite this article as: S.S. Hossain, P.K. Roy, Waste rice husk ash derived sol: A potential binder in high alumina refractory castables as a replacement of hydraulic binder, Journal of Alloys and Compounds, https://doi.org/10.1016/j.jallcom.2019.152806

diffractometer equipped with Cu-kα (1.5406 Å) radiation and Ni filter, the step size of 0.02° in the range of 10° to 80°. Surface morphology of the sintered castables was observed by the scanning electron microscopy (SEM) (FEI, Nova Nano SEM 450, Netherlands). The bulk density (BD) and apparent porosity (AP) of the fired castables were measured according to ASTM C20. Cold modulus of rupture (CMoR) of the fired castable and cold compressive strength (CCS) of the green and fired castable specimens was done according to ASTM C133 (UTM, H10KL-I0129). The hot modulus of rupture (HMoR) of fired castable specimens was determined at 1400 °C according to ASTM C583-10 in a HMoR furnace (Bysakh & Co, Kolkata, India). Thermal shock resistance (TSR) of the fired castable samples was examined by the measurement of CCS values after repetitively air quenching from 1200 °C to ambient temperature. The fired castable specimens were heat-treated at 1200 °C for 15 min and air quenching at room temperature for 10 min. This event was repeated and CCS was measured at a regular interval of 2 cycles. For BFS corrosion resistance, the central groove (10 mm diameter and 15 mm height) of the fired castable blocks were used and BFS powder was poured into the groove. The melting was done in a muffle furnace at 1500 °C for 30 h. The blocks were then cut into vertically by diamond cutter and the castable-BFS interface was examined by SEM and energy dispersive X-ray (EDX)-mapping techniques.

3. Results and discussion

3.1. Characterization of silica sol

The waste RHA derived sol is appeared in white color. The pH value of the sol is about ~9. When the sol is heat-treated above at 1200 °C/1 h, it is given around 30 wt% of solid content. The discussion about the dry sol is reported in our previous publication [28]. It retains about 99.32 wt% of amorphous SiO_2.

The shape, size and internal structure of the silica present in sol are deeply examined by the TEM analysis, which is displayed in Fig. 2. It is observed that the silica particles are closely spherical in shape and the average size is around 22 nm. It is also seen that the nano particles are enormously agglomerated. It may be attributed due to existing of silicon-oxygen bridge bonds in the network [29]. The surface to volume ratio of these nano particles is high. It may be ascribed to the strong attractive cohesive forces between the SiO_2 particles, may be another reason of agglomeration [30]. The selective area electron diffraction (SAED) pattern of the sol specifies that the structure of present silica in the sol is amorphous in nature due to the deficiency of intensities rink in the pattern.

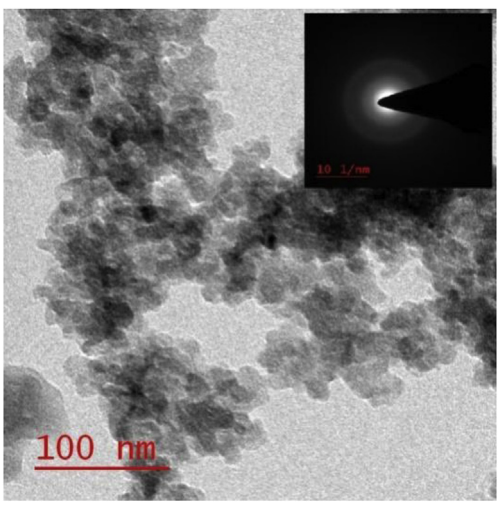

Fig. 2. TEM analysis of RHA derived sol.

Waste RHA derived high purity nano size amorphous silica containing sol is environmentally and economically benign. Moreover, alkali extraction route derived silica sol from RHA is economical due to low synthesis temperature (90 °C) and inexpensive raw materials. It has no tendency to generate any greenhouse gases like CO_2 during the sol extraction as the waste RHA is already burn in boiler. Other possible gases like hydrochloric (HCl ↑) or chlorine (Cl ↑) are transformed into NaCl through the reaction 2. Table 3 shows the cost estimation of silica sol production per litre through the alkali extraction method from RHA as ingredient. Estimated cost of 30 wt% solid (~22 nm average silica particles) containing sol is around 9.35$ per litre. Subsequently, the cost of commercially available silica sol in market is 0.5$ to 52$ per litre, depends on the solid content, purity and particle size of silica [31,32]. It is concluded that this waste derived high purity (99.32%) silica sol from alkali extraction route is eco-friendly and cheaper compare to its present available aspects.

3.2. Characterization of mullite

Fig. 3 illustrates the DTA-TGA curve of the dried mixture containing stoichiometric (3:2) amount of reactive alumina and silica (~30 wt% solid containing sol) to evaluate the most possible mullite formation mechanism. The TGA curve depicts two distinct weight losses from room temperature to 510 °C. The first weight loss (~4.5%) up to 170 °C is observed due to the elimination of absorbed water from the mixture. Next weight loss (~6%) at 230 °C–510 °C may be attributed due to the breaking of Si–OH bonds, presented in silica sol [33]. Consequently, both weight losses are associated with endothermic peaks in DTA curve. Further, no weight changes are detected in TGA curve up to 1300 °C. However, first exothermic peak at 770 °C–940 °C in DTA curve may be related to the transformation of amorphous to crystallization of sol containing nano-silica [34]. The next exothermic peak is detected at around 1030 °C. It may be ascribed due to the combination effects like transformation of alumina phase and the formation of Al–Si spinel or nucleation of mullite phase (first step mullite) [35,36]. At high temperature, wide range of exothermic peak at 1110 °C–1300 °C (center at 1250 °C) may be indicated the crystallization reactions of two step mullite [37,38].

Fig. 4 depicts the XRD pattern of 1100 °C, 1200 °C and 1250 °C sintered mixture mass of 3:2 M ratio reactive alumina and silica (~30 wt% solid containing sol). It reveals that at 1100 °C and 1200 °C, amorphous silica containing sol completely transforms into cristobalite (JCPDC card number: 76–0937) and some mullite (JCPDS card number: 06–0258) phases. The mullitization is started above 1000 °C through the diffusion reaction of reactive alumina and nano silica, as shown in DTA curve at 1030 °C (Fig. 3). This

Table 2
Chemical composition of the ingredients.

Compound	Tabular alumina (wt.%)	CAC (wt.%)	Blast furnace slag (wt.%)
SiO_2	0.76	0.30	35.42
Na_2O	0.17	0.80	–
CaO	–	18.10	40.67
Fe_2O_3	0.49	0.20	0.45
MgO	–	0.40	6.83
P_2O_5	–	–	0.13
Al_2O_3	98.16	80.20	14.52
S	–	–	1.23
MnO	–	–	0.73
TiO_2	0.42	–	–

Please cite this article as: S.S. Hossain, P.K. Roy, Waste rice husk ash derived sol: A potential binder in high alumina refractory castables as a replacement of hydraulic binder, Journal of Alloys and Compounds, https://doi.org/10.1016/j.jallcom.2019.152806

Table 3
Cost estimation of silica sol (~30% solid) synthesis per litre using RHA as source.

Raw materials used			Energy			Labour cost + others
Name	Cost per kg	Unit price[a]	Name	Cost per kg	Unit price	
Rice husk ash	0	0	Magnetic stirring and oven	(0.18 + 0.18) $	0.15 $ per KW	
NaOH pellet	2.94 $	5.2 $ per kg				
HCl solution (1 N)	4.05 $	5.4 $ per L				
6.99 $			0.36 $			2 $
Total extraction cost of silica sol per litre ~ 9.35 $						

[a] https://www.lobachemie.com/flipbooks.

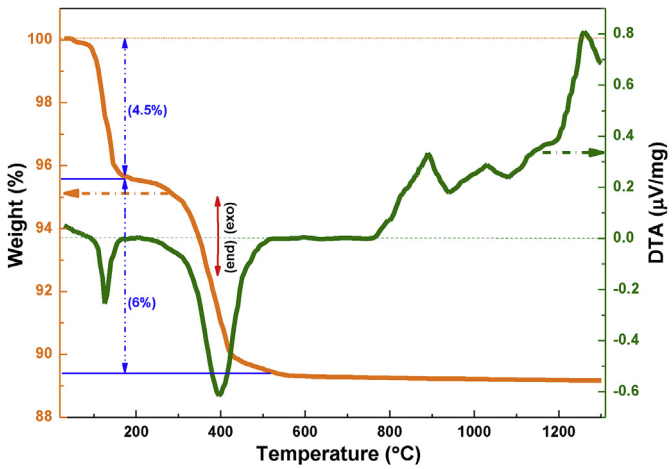

Fig. 3. DTA-TGA curve of reactive alumina and sol mixture.

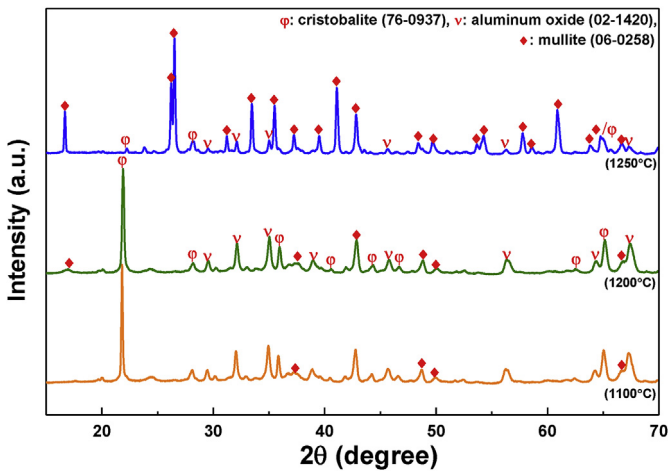

Fig. 4. XRD pattern of1100 °C, 1200 °C and 1250 °C sintered mixture mass of reactive alumina and sol.

diffusion reaction may be occurred on the surface of alumina particles after accruing the required activation energy (1100 ± 100 kJ/mol) due to huge size difference of reactive alumina (<1 μm) and nano silica (~22 nm) particles [36]. Therefore, precipitation of mullite starts on the surface of alumina particles. A schematic representation of the diffusion reaction of reactive alumina and sol containing nano silica is shown in Fig. 5. At high temperature (1250 °C), significant mullite peaks are emerged, whereas, numbers of cristobalite and alumina peaks are disappeared or intensity is reduced in XRD pattern (Fig. 4). It's may be happened due to more amount of Al^{3+} ions from reactive alumina are diffused through the mullite phase to form further stable mullite formation with nano silica. It is attributed to a strong exothermic peak in DTA curve (Fig. 3) at around 1250 °C. The presence of large amount of nano sized silica in the system acts as nucleation centers for stable mullite formation. Most intense diffraction peak at ~26.40° for 1250 °C sintered sample is corresponding to the mullite formation and it is dominating phase in the system [38]. The formed mullite grains are continually grown and produced a diffusion barrier between the reactive alumina and nano silica. Later, it is hindered the further mullite formation in the matrix. Therefore, some residual amounts of silica and alumina phases are present in between the mullite phases, and their existence is detected in XRD pattern (Fig. 4) of 1250 °C sintered sample. To complete further mullite phase formation, higher temperature is required. It provides more activation energy to migrate Al^{3+} ions through the barrier. However, significant amount of mullite phase is formed at 1250 °C (Fig. 4) in the mixture of reactive alumina and sol and it may confirm that the firing temperature for mullite formation in this system is 1250 °C or higher.

Fig. 6 shows the SEM micrograph of 1100 °C and 1250 °C sintered mixture of reactive alumina and sol. From the micrograph, it is clearly observed that the nano size mullite grains are nucleated on the surface. The number and size of mullite grains are increased with the increasing of sintering temperature from 1100 °C to 1250 °C. However, formed mullite grains are mostly spherical in shapes. It may be happened due to high size differences of the reaction constitutions. Thus, the growth in particular direction may be inhibited and the spherical shaped mullite is formed.

3.3. Characterization of castable

The castable samples with different composition are prepared using RHA derived sol as a binder and ten specimens of each composition are fabricated for appropriate results. The samples are sintered at 1400 °C, 1500 °C and 1550 °C. It is lower temperature than the sintering temperature of conventional no cement castable [39,40]. No deformity on shape and dimensions is detected for all the sintered castable samples, as exhibits in Fig. 1.

The phase analysis of refractory castable is important to identify the existent of any low melting impurity phase in the matrix of castable. It commonly deteriorates the properties and performance at high temperature. Fig. 7 depicts the XRD patterns of some selective sintered castable specimens. It can be identified that the corundum is a major crystalline phase for all the fired samples.

However, some calcium aluminum oxide phases are identified in the XRD pattern (Fig. 7) of s-0 samples. On the other hand, RHA derived silica sol containing samples (s-2, s-3 and s-4) are retaining some in-situ mullite peaks in the XRD pattern (Fig. 7) as a minor phase. This mullite is developed through the diffusion reaction of reactive alumina and sol containing nano silica at above 1200 °C, as

Please cite this article as: S.S. Hossain, P.K. Roy, Waste rice husk ash derived sol: A potential binder in high alumina refractory castables as a replacement of hydraulic binder, Journal of Alloys and Compounds, https://doi.org/10.1016/j.jallcom.2019.152806

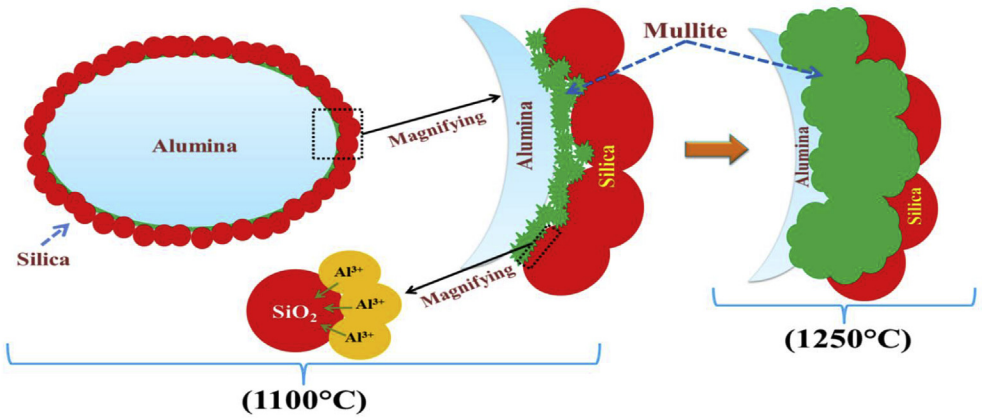

Fig. 5. Schematic representation of mullite formation reaction mechanism of reactive alumina and sol containing nano silica.

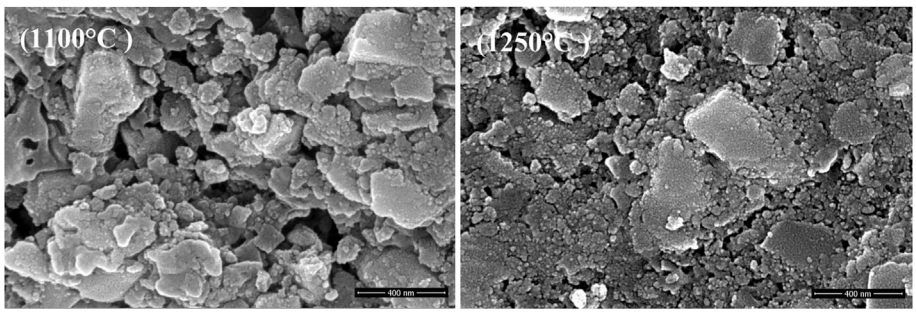

Fig. 6. SEM micrograph of 1100 °C and 1250 °C sintered mixture of reactive alumina and sol.

discussed in the previous section (characterization of mullite). Theoretically, 2 wt% (s-1), 4 wt% (s-2), 5 wt% (s-3) and 6 wt% (s-4) nano silica containing high alumina castable are produced maximum 7.10 wt%, 14.20 wt%, 17.75 wt% and 21.30 wt% in-situ mullite ($3Al_2O_3 \cdot 2SiO_2$), respectively, in the matrix. Moreover, some unreacted silica peaks are detected in 6 wt% of nano silica containing (s-4) castable specimens. So, further addition of silica sol in the composition of castable may dilute the high temperature properties due to the formation of free silica in the matrix.

The behaviors of the sintered ceramic bodies are not only influenced by the present phase but also very much dependent on the developed microstructure like distribution of present phases, sinterability, and amount of pores [41]. The SEM images of the fractured cross-sectional surfaces of the sintered castable (s-0 and s-3) specimens are depicted in Fig. 8. It is notified that the cement containing (s-0) and sol containing (s-3) specimens are demonstrated slight different microstructures. s-0 specimen shows lower grade of densification with some pores (P) on the surface at 1400 °C. However, at 1550 °C sintered s-0 specimen exhibits a compacted structure without any magnificent pores. High magnification image of s-0 (1550 °C) sample shows some liquid phases (L) in the interfaces of corundum (C) grains. Hence, liquid phase sintering is attributed for CAC containing samples. Conversely, sol containing s-3 specimens retain a uniform rigid morphology. It may be ascribed due to the sol with nano silica particles. It has great sinterability characteristic at high temperature due to the high surface area of nano silica particles. It helps to react with alumina sources and forms a continuous in-situ mullite (M) matrix. The needle like mullite grains are formed in the castable network, as observed in high magnification image. At high temperature, more activation energy helps to react alumina with nano silica and forms nano size mullite in a particular direction. Therefore, low temperature (1250 °C) formed spherical mullite grains (Fig. 6) are transformed into needle shape mullite grains at 1550 °C (Fig. 8).

Table 4 depicts the mean value of BD and AP of the fired castable specimens. It can be observed that the RHA derived sol containing samples show slight lower value of AP than CAC containing s-0 sample sintered at 1400 °C. Sol containing nano silica is started to form significant amount of in-situ mullite phase after 1200 °C in the castable (as shown in Fig. 4). It may enhance the densification through the development of continuous bonding matrix in the aggregates. Additionally, nano particles improve the packing efficiency of refractory castable by filling inter-aggregates pores of castable [7]. 6 wt% (3 wt% sol + 3 wt% dry sol) silica containing s-4 sample exhibits lowest porosity. It may be ascribed due to presence of unreacted nano silica at 1400 °C (Fig. 7). This free nano silica forms a viscous phase in-between the refractory aggregates and fills the pores. However, the porosity effect doesn't significantly affect the BD of the castable. It may be due to high density CAC (~3340 kg/m^3) is replaced by the low density material (silica, ~2200 kg/m^3) or formation of low density phase, i.e., mullite (~3100 kg/m^3). The AP values are reduced and BD is improved with increasing the sintering temperature from 1400 °C to 1500 °C or 1550 °C due to accelerate different sintering mechanism and shrinking of pores volume. s-0 sample shows more reduction of AP (~10.17%) value with increasing the firing temperature from 1400 °C to 1550 °C. It may be attributed due to the formation of low eutectic phases above 1400 °C (Fig. 8). This phases are introduced the liquid phase sintering in the castable (s-0 and s-1) and reduced the AP values. The formation of more amount of mullite phase (Fig. 8) in the system with increasing temperature is assisted for reduction of AP and enhancing of BD for sol containing samples (s-2 to s-4).

Please cite this article as: S.S. Hossain, P.K. Roy, Waste rice husk ash derived sol: A potential binder in high alumina refractory castables as a replacement of hydraulic binder, Journal of Alloys and Compounds, https://doi.org/10.1016/j.jallcom.2019.152806

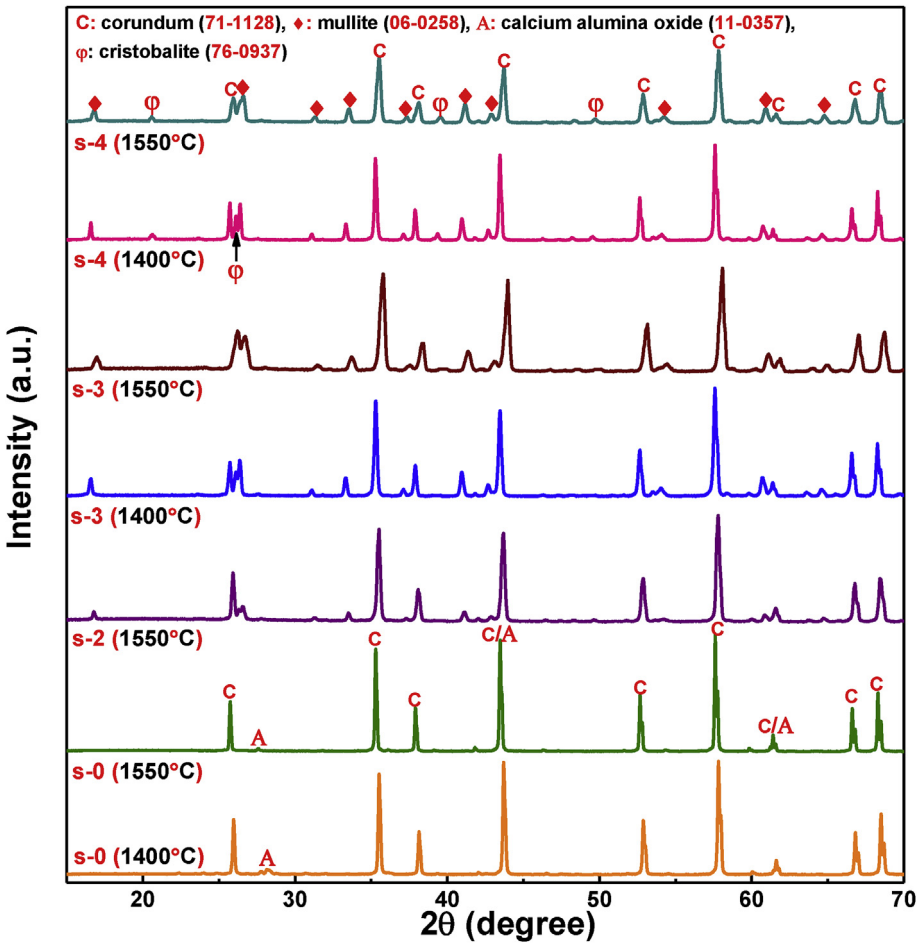

Fig. 7. XRD pattern of sintered castable specimens.

The green CCS values of the castable specimens after drying at 80 °C are shown in Fig. 9(a). CAC containing samples (s-0 and s-1) show good green strength than sol containing samples (s-2, s-3 and s-4). It may be happened due to the formation of CAH_{10}, C_3AH_6 and C_2AH_8 phases in the castable matrix through the hydration of CAC containing phases like CA, CA_2 and $C_{12}A_7$ [18]. These hydration phases are provided an interlocked network in the system of castable and help to bind the aggregates. It delivers the green strength or setting behavior of the castable. However, sol containing specimens also display the sustainable strength values. The sol retains hydrated silicon (Si—OH) particles. During drying of castable, the hydroxyl group from the sol is removed as a water vapors and free silanol groups (Si—OH) is transferred into siloxane bond (Si—*O*—Si) through Eq. (3). It forms 3D networks of Si—*O*—Si bonds in the castable matrix. It can be encapsulated the solid aggregates and provided the green strength of the castable. Fig. 9(b) depicts the schematic representation of gelation mechanisms of nano silica sol. It helps to understand the reason behind the green strength of sol containing castable specimens.

$$-Si-OH+OH-Si- \;=\; -Si-O-Si-+H-O-H\uparrow \qquad (3)$$

Fig. 10(a) and (b) illustrates the CCS and CMoR values of castable specimens after sintering, respectively. The strength values of the castable specimens are improved with the sintering temperature. It may be attributed due to the hydration or week sol bonds are substituted through the robust ceramic bonds. Subsequently, both strength values of CMoR and CCS are expressively improved with the addition of sol in the place of CAC (s-1 and s-2) or calcined alumina (s-3 and s-4). Sol introduces nano silica in the system, and fills the inter-aggregate void. Sol generates highly active SiO_2 particles which are favorable to the reaction with reactive alumina for the formation of in-situ mullite. This mullite phase introduces a network into the castable matrix. The reduction of void volume and introduction of mullite network enhances the strength values of the castable with sol incorporation in the system. However, CCS and CMoR are improved with increasing the sintering temperature due to increase in sinterability characteristics of the castable. It is also observed that the presence of free silica in s-4 sample does not degrade the room temperature strength values.

The analysis of hot flexural strength of castable specimens is performed at 1400 °C. The HMoR values of some selective castable specimens (s-0, s-2, s-3 and s-4) sintered at 1400 °C and 1550 °C are illustrated in Fig. 11. 1400 °C sintered specimens show low value of HMoR, it may be due to lack of densification (Table 4). The porosity in the castable introduces number of crack generate sites, which aid to reduce the strength value. However, 1550 °C sintered samples show above 10 MPa of HMoR values, which is considered for application in castable refractories [42]. The development of uniform dense microstructure may be the reason of improving HMoR values. Subsequently, silica sol containing specimens are exhibited higher values of HMoR due to introduce of fine mullite particles in the castable matrix. The formation of mullite is enhanced the sintering mechanisms and developed strength. The mullite (melting point ~1840 °C) has higher ability to resist the braking forces than

Please cite this article as: S.S. Hossain, P.K. Roy, Waste rice husk ash derived sol: A potential binder in high alumina refractory castables as a replacement of hydraulic binder, Journal of Alloys and Compounds, https://doi.org/10.1016/j.jallcom.2019.152806

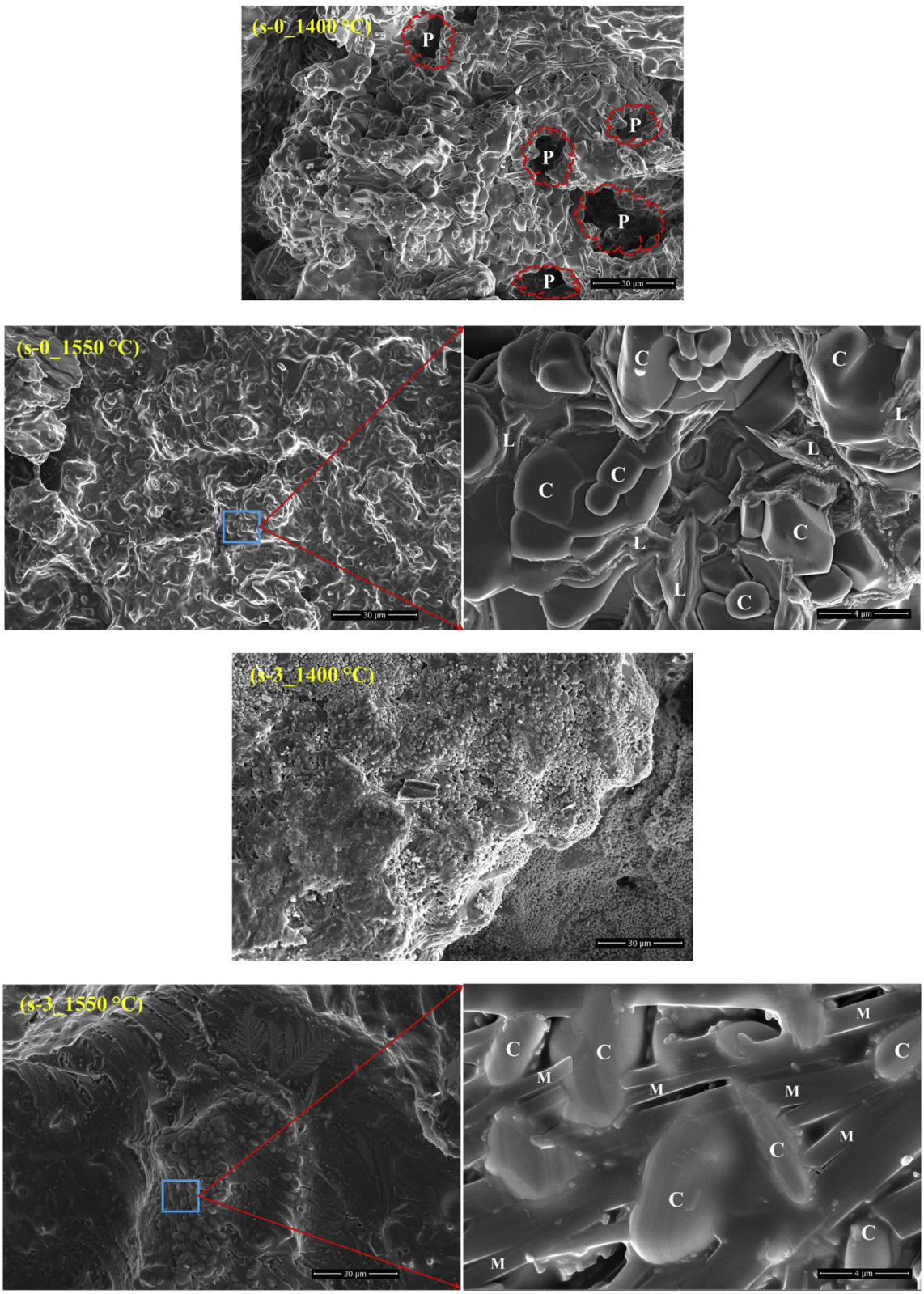

Fig. 8. SEM micrographs of the fractured cross sectional surfaces of sintered refractory castables.

calcium aluminate phases at high temperature. The CAC containing specimens have a possibility to form low melting phase like $C_{12}A_7$ (~1400 °C) in the castable system. Consequently, 6 wt% (s-4) sol containing castable specimen shows slightly lower value of HMoR than 5 wt% (s-3) containing specimen. It may be happened due to presence of free nano silica, which may form viscous phases at high temperature and reduce the HMoR value of the castable.

4 wt% CAC containing (s-0) and 5 wt% silica containing (s-3)

Please cite this article as: S.S. Hossain, P.K. Roy, Waste rice husk ash derived sol: A potential binder in high alumina refractory castables as a replacement of hydraulic binder, Journal of Alloys and Compounds, https://doi.org/10.1016/j.jallcom.2019.152806

Table 4
Apparent porosity and bulk density of sintered castable samples.

Samples	Apparent porosity (%)						Bulk density (gm/cc)					
	1400 °C		1500 °C		1550 °C		1400 °C		1500 °C		1550 °C	
	Mean	s.d.	Mean	s.d.	Mean	s.d.	Mean	s.d.	Mean	s.d.	Mean	s.d.
s-0	17.78	1.02	10.95	0.68	7.61	0.54	2.73	0.02	2.83	0.04	2.90	0.03
s-1	15.17	0.95	11.27	0.83	7.57	0.62	2.75	0.02	2.82	0.04	2.91	0.05
s-2	14.27	0.79	10.08	0.66	7.22	0.74	2.76	0.03	2.81	0.03	2.92	0.04
s-3	13.11	0.92	8.75	0.78	6.49	0.45	2.77	0.03	2.82	0.03	2.91	0.03
s-4	10.43	0.86	7.23	0.84	5.41	0.53	2.76	0.03	2.84	0.04	2.93	0.04

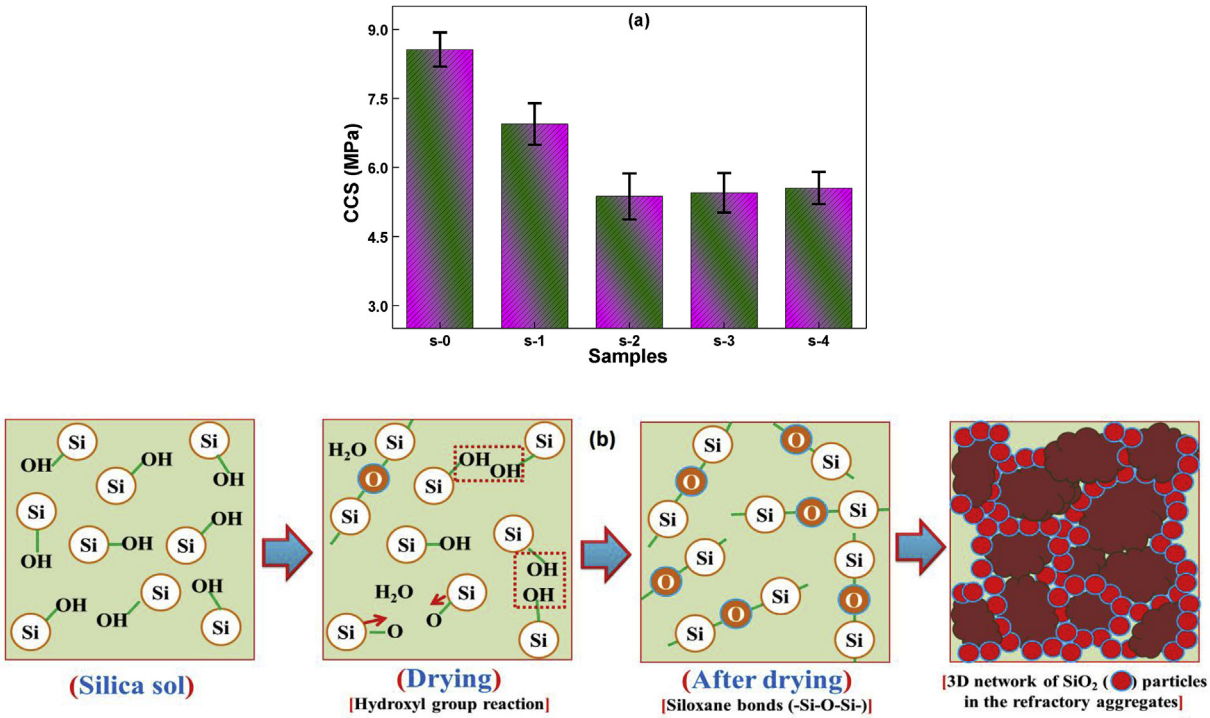

Fig. 9. (a) Green CCS values of castable specimens after drying at 60 °C and (b) gelation mechanisms of nano silica sol [10]. (For interpretation of the references to color in this figure legend, the reader is referred to the Web version of this article.)

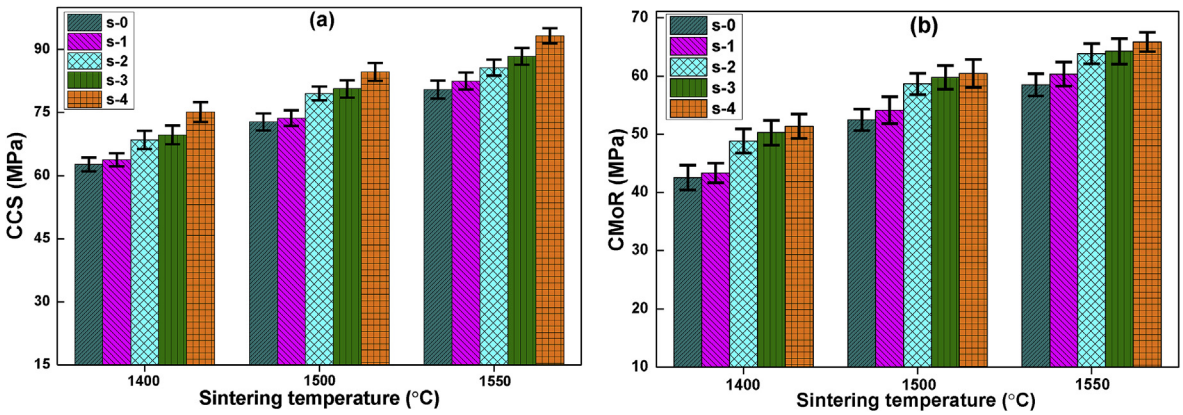

Fig. 10. (a) CCS and (b) CMoR values of sintered castable specimens.

samples (highest HMoR among all sol containing samples) are taken for TSR evaluation. Fig. 12 displays the percent of retention CCS values of the respective samples as a function of undergoing number of thermal cycles.

s-0 specimen shows a gradually degradation of CCS values with the thermal fatigue. It may be due to the generation of subcritical cracks in the castable system during thermal cycle because of huge temperature differences (~1170 °C) and the cracks continuous propagate with repetitively thermal shock [43]. The retaining strength of s-0 sample is ~59% of its original strength value after 10th thermal cycles. The silica sol containing s-3 sample initially shows a slightly higher degradation rate than s-0 sample. The

Please cite this article as: S.S. Hossain, P.K. Roy, Waste rice husk ash derived sol: A potential binder in high alumina refractory castables as a replacement of hydraulic binder, Journal of Alloys and Compounds, https://doi.org/10.1016/j.jallcom.2019.152806

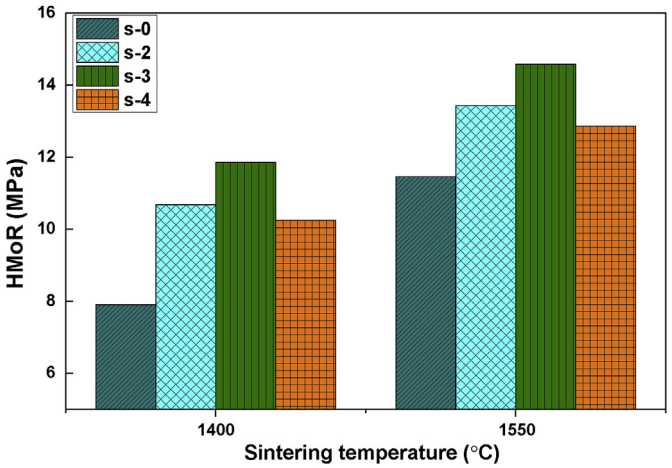

Fig. 11. HMoR values of castable specimens at 1400 °C.

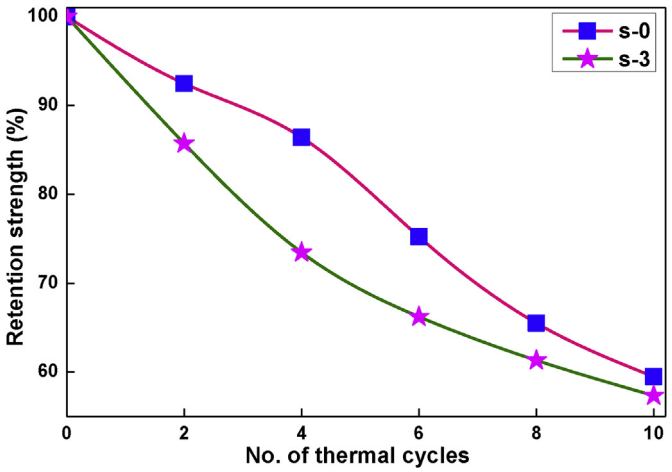

Fig. 12. Retention of CCSvaluesof s-0 and s-3 specimens after undergoing number of thermal cycle.

mismatch of thermal expansion coefficient between alumina (~8.1 × 10^{-6}/°C) and mullite (~5.4 × 10^{-6}/°C) particles, introduces a higher concentration of stresses in the system. It aids to generate number of micro-cracks; results crack propagation in the matrix. Fig. 13 depicts the surface morphology of s-3 specimen after 6th thermal shock cycles and its shows that the numbers of micro cracks are generated on the surface. This may be the reason of rapid reduction in the strength retainment capacity of s-3 sample. However, the strength degradation rate of s-3 is decreased after 6th thermal cycles and after 10th cycles it is retained around ~57% of its initial strength value.

s-3 specimen after firing at 1550 °C is exhibited optimum properties without free silica among other sol containing specimens. This composition (s-3) and 4 wt% CAC containing (s-0) specimen are selected for blast furnace slag (BFS) corrosion test. The composition of BFS is tabulated in Table 2. In the BFS, the major compounds are CaO, SiO_2 and Al_2O_3 and contains around 40.67 wt %, 35.42 wt% and 14.52 wt%, respectively. BFS's melting temperature is above 1400 °C. The corrosion test is performed at 1500 °C for 30 h in an air atmosphere and the test schematic is represented in Fig. 14. The corrosion region and the depth of slag penetration are observed by the SEM micrograph and EDX-mapping at castable-slag interface, as shown in Fig. 15 s-0 sample exhibits a clear corrosion region in the interface of castable-slag. The presence of

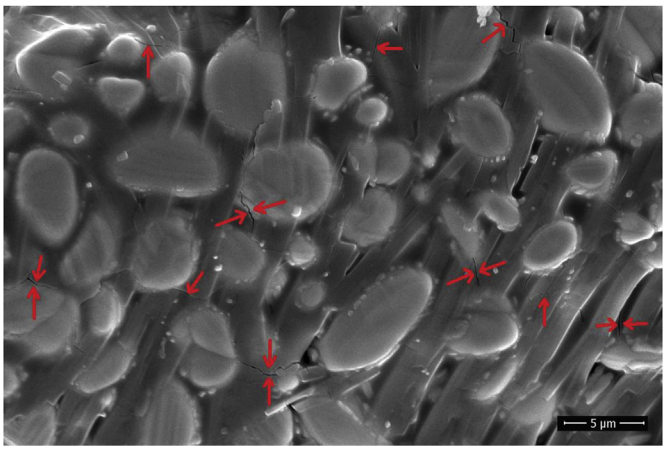

Fig. 13. SEM micrograph of s-3 specimen after 6th thermal shock.

fused phases at high temperature have been reacted more potentially with the slag melt and permitted to the slag penetration in the castable. The liquid phases are unable to build the barrier for slag penetration. Therefore, different ions from slag easily transfer into castable. EDX-mapping image for s-0 (Fig. 15) shows the Ca ion migration from the slag to castable. It is clearly observed that the ion concentration of Ca in the corrosion region is higher than non-corrosive region in the castable. The slag penetration depth of s-0 sample is around 150 μm after 30 h of heat-treatment. Oppositely, s-3 shows a superior corrosion resistance behavior due to highly dense microstructure (Fig. 8) and phase purity (Fig. 7). The absent of any low melting phases like free silica helps to enhance the slag corrosion resistance. Additionally, the formation of in-situ mullite phase (~17.75 wt% theoretically) in the system retains the orthorhombic crystal structure, which has oxygen vacancies and it is capable to arrest many cations like Mg, Ti, Fe, etc [39]. The developed in-situ mullite therefore, adsorbs many cations from the slag melt and changes the viscosity and composition of the slag. It is resulted in the further reduction of slag penetration [39]. Therefore, s-3 specimen shows the low density of Ca ion concentration (Fig. 15) in the castable and the depth of penetration is around ~65 μm.

The comparable studies on the different properties of waste RHA derived sol bonded castable (s-3) with convention silica bonded systems are shown in Table 5. Though, the composition of refractory aggregates, different additives and particle size distribution are not same with this study. It can be observed that evaluated properties of s-3 sample are suitable according to the other sources of silica bonded castables. Thus, waste RHA derived sol has been a great potential as a sustainable source of silica sol for replacing the conventional silica sources in cement free unshaped refractory.

4. Conclusions

Stable silica sol is prepared from waste RHA through alkali extraction route. The sol is contained 30 wt% of nano amorphous silica with average particle size 22 nm and estimated cost of per litre sol is around 9.35 $. No cement high alumina refractory castable specimens are prepared by the replacing of calcium alumina cement through the RHA derived sol. Densification, cold and hot strength, and corrosion resistance of the castable specimens are improved with the incorporation of sol. Sol containing nano silica is reacted with different alumina sources in the castable and started formation of in-situ mullite at above 1200 °C. 5 wt% (s-3) silica containing 1550 °C sintered sample shows good physico-

Please cite this article as: S.S. Hossain, P.K. Roy, Waste rice husk ash derived sol: A potential binder in high alumina refractory castables as a replacement of hydraulic binder, Journal of Alloys and Compounds, https://doi.org/10.1016/j.jallcom.2019.152806

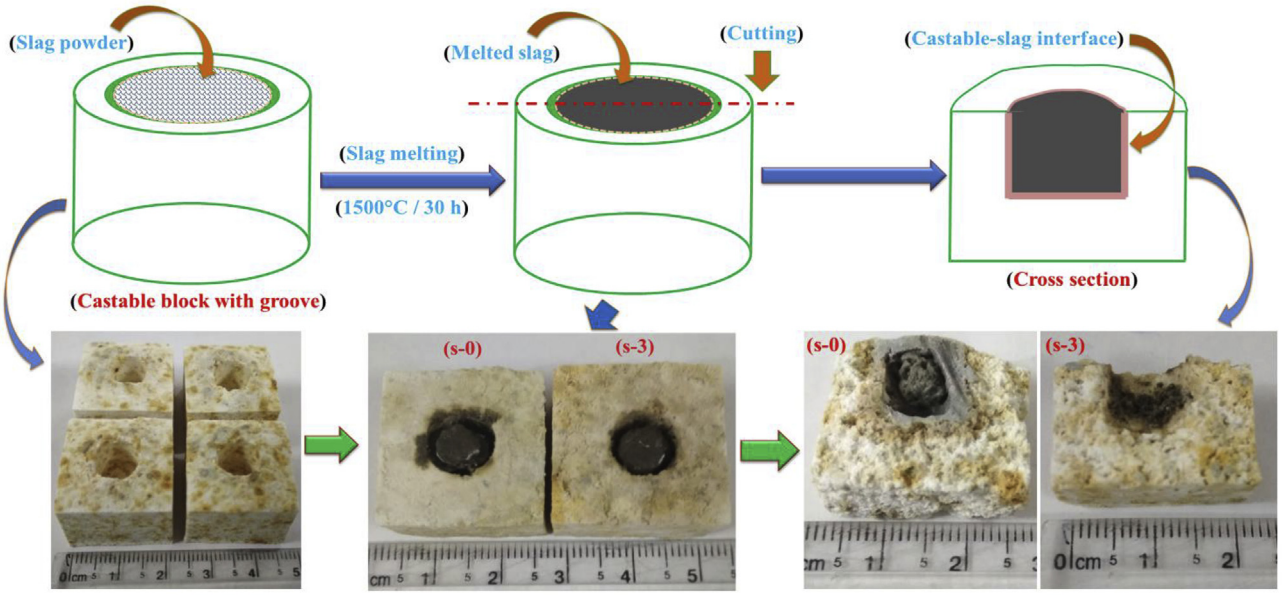

Fig. 14. Schematic representation of static corrosion test.

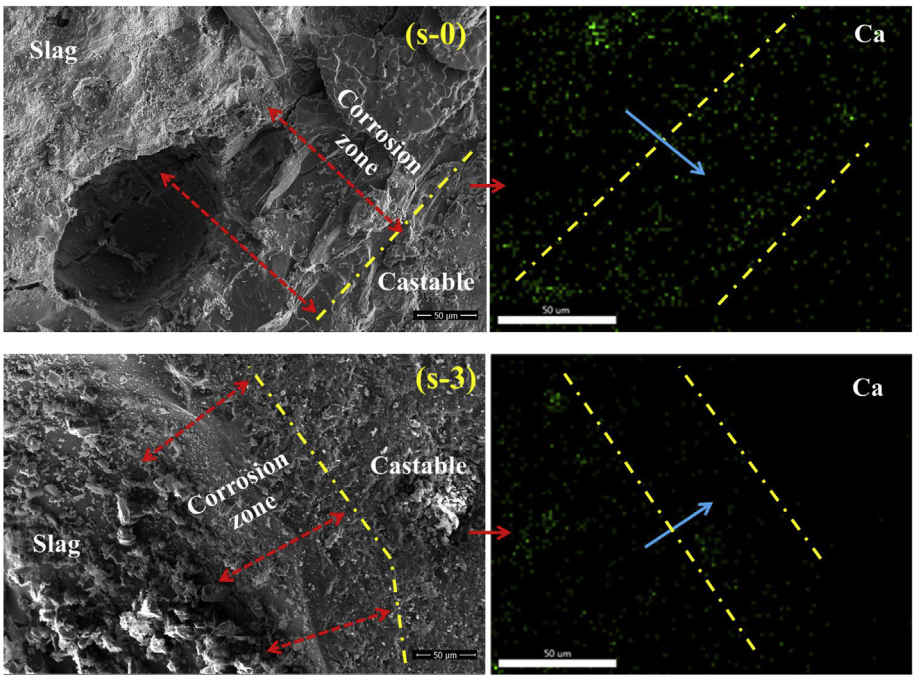

Fig. 15. SEM photomicrographs and EDX-mapping analysis of the castable-slag interface after BFS corrosion test.

Table 5
Physico-mechanical properties of waste RHA derived sol bonded castable against other source of silica sol bonded castables.

Properties	Our study (s-3)	Colloidal silica [1]	Silica sol [44]	Colloidal silica [8]
Firing temperature (°C)	1550	1600	1650	1400
Bulk density (gm/cc)	2.91	3.05	3.17	–
Strength after fired (MPa)	88 (CCS), 64 (CMoR)	110 (CCS)	27 (CMoR)	32 (CMoR)
HMoR at 1400 °C (MPa)	14	9	–	10
TSR after 8th cycle (MPa)	53	64	–	–

Please cite this article as: S.S. Hossain, P.K. Roy, Waste rice husk ash derived sol: A potential binder in high alumina refractory castables as a replacement of hydraulic binder, Journal of Alloys and Compounds, https://doi.org/10.1016/j.jallcom.2019.152806

mechanical properties without retaining unreacted free silica. The evaluated properties of castable are compared with the convention colloidal silica bonded castable and good matching is observed. The absence of any liquid phase formation (free silica) and superior properties of waste derived sol containing cement free castable system is able to be useful for high temperature applications like steel ladles and blast furnaces lining.

Acknowledgments

The authors are grateful to the MHRD, New Delhi, India for the financial assistance and also wish to thank IIT (BHU) & CIFC (IIT-BHU) for providing facilities.

References

[1] A.K. Singh, R. Sarkar, High alumina castables: a comparison among various sol-gel bonding systems, J. Australas. Ceram. Soc. (2017), https://doi.org/10.1007/s41779-017-0067-1.
[2] W.E. Lee, W. Vieira, S. Zhang, K.G. Ahari, H. Sarpoolaky, C. Parr, Castable refractory concrete, Int. Mater. Rev. 46 (3) (2001) 145–167.
[3] C. Parr, J. Pelletier, C. Wöhrmeyer, C. Zetterstrom, A review of bond systems for monolithic castable refractories, Refract. Worldforum 7 (2005) 63–70.
[4] M.N. Khezrabad, M.A.L. Braulio, V.C. Pandolfelli, F. Golestani-Fard, H.R. Rezaie, Nanobonded refractory castables, Ceram. Int. 39 (2013) 3479–3497.
[5] A.P. Luza, L.B. Consoni, C. Pagliosa, C.G. Aneziris, V.C. Pandolfelli, MgO fumes as a potential binder for in situ spinel containing refractory castables, Ceram. Int. 44 (2018) 15453–15463.
[6] S.J.S. Lopes, A.P. Luz, D.T. Gomes, V.C. Pandolfelli, Self-flowing high-alumina phosphate-bonded refractory castables, Ceram. Int. 43 (2017) 6239–6249.
[7] J. Roy, S. Chandra, S. Maitra, Nanotechnology in castable refractory, Ceram. Int. (2019), https://doi.org/10.1016/j.ceramint.2018.09.261.
[8] A.P. Luz, S.J.S. Lopes, D.T. Gomes, V.C. Pandolfelli, High-alumina refractory castables bonded with novel alumina-silica-based powdered binders, Ceram. Int. 44 (2018) 9159–9167.
[9] O.B. Montes, M. Álvarez, A.H.D. Aza, P. Pena, C. Baudín, The main role of silica-Based cement free binders on the microstructural evolution and mechanical behaviour of high alumina castables, J. Eur. Ceram. Soc. 38 (2018) 4137–4148.
[10] M. R Ismael, R.D. Anjos, V.C. Pandolfelli, Colloidal silica as a nano structured binder refractory castables, Refract. Appl. News 11 (4) (2006) 16–20.
[11] M.R. Ismael, R. Salomao, V.C. Pandolfelli, Colloidal silica bonded refractory castables: optimization of the particle size distribution, Refract. Appl. News 13 (2008) 1.
[12] H. Schneider, J. Schreuer, B. Hildmann, Structure and properties of mullite – are view, J. Eur. Ceram. Soc. 28 (2008) 329–344.
[13] H.M. Lim, J. Lee, J.H. Jeong, S.G. Oh, S.H. Lee, Comparative study of various preparation methods of colloidal silica, Engineering 2 (2010) 998–1005.
[14] E.D.E.R. Hyde, A. Seyfaee, F. Neville, R.M. Atanasio, Colloidal silica particle synthesis and future industrial manufacturing pathways: a review, Ind. Eng. Chem. Res. 55 (2016) 8891–8913.
[15] R. Pode, Potential applications of rice husk ash waste from rice husk biomass power plant, Renew. Sustain. Energy Rev. 53 (2016) 1468–1485.
[16] D. An, Y. Guo, Y. Zhu, Z. Wang, A green route to preparation of silica powders with rice husk ash and waste gas, Chem. Eng. J. 162 (2010) 509–514.
[17] S. Mor, K. Chhoden, K. Ravindra, Application of agro-waste rice husk ash for the removal of phosphate from the wastewater, J. Clean. Prod. 129 (2016) 673–680.
[18] S. Mor, C.K. Manchanda, S.K. Kansal, K. Ravindra, Nano silica extraction from processed agricultural residue using green technology, J. Clean. Prod. 143 (2017) 1284–1290.
[19] S.M.S. Kazmi, S. Abbas, M.J. Munir, A. Khitab, Exploratory study on the effect of waste rice husk and sugarcane bagasse ashes in burnt clay bricks, J. Build Eng. 7 (2016) 372–378.
[20] S.K. Hubadillah, M.H.D. Othman, A.F. Ismail, M.A. Rahman, J. Jaafar, Y. Iwamoto, S. Honda, M.I.H.M. Dzahir, M.Z.M. Yusop, Fabrication of low cost, green silica based ceramic hollow fibre membrane prepared from waste rice husk for water filtration application, Ceram. Int. (2018), https://doi.org/10.1016/j.ceramint.2018.03.067.
[21] S.S. Hossain, L. Mathur, P.K. Roy, Rice husk/rice husk ash as an alternative source of silica in ceramics: a review, J. Asian Ceram. Soc. (2018), https://doi.org/10.1080/21870764.2018.1539210.
[22] S. Songa, H.B. Chob, H.T. Kim, Surfactant-free synthesis of high surface area silica nanoparticles derived from rice husks by employing the Taguchi approach, J. Ind. Eng. Chem. 61 (2018) 281–287.
[23] J.A.S. Costa, C.M. Paranhos, Systematic evaluation of amorphous silica production from rice husk ashes, J. Clean. Prod. 192 (2018) 688–697.
[24] S. Sembiringa, W. Simanjuntak, P. Manurunga, D. Asmia, I.M. Low, Synthesis and characterisation of gel-derived mullite precursors from rice husk silica, Ceram. Int. 40 (2014) 7067–7072.
[25] M.F. Serra, M.S. Conconi, M.R. Gauna, G. Suáreza, E.F. Aglietti, N.M. Rendtorff, Mullite ($3Al_2O_3 \cdot 2SiO_2$) ceramics obtained by reaction sintering of rice husk ash and alumina, phase evolution, sintering and microstructure, J Asian Ceramic Soc 4 (2016) 61–67.
[26] L. Fernandes, R. Salomão, Preparation and characterization of mullite-alumina structures formed "in situ" from calcined alumina and different grades of synthetic amorphous silica, Mater. Res. 21 (3) (2018), 20170783, https://doi.org/10.1590/1980-5373-MR-2017-0783.
[27] S.S. Hossain, P.K. Roy, Studies on physical and dielectric properties of bio-wastes derived synthetic wollastonite, J. Asian Ceram. Soc. 6 (3) (2018) 289–298.
[28] S.S. Hossain, L. Mathur, A. Bhardwaj, P.K. Roy, A facile route for the preparation of silica foams using rice husk ash, Int. J. Appl. Ceram. Technol. (2019) 1–9, https://doi.org/10.1111/ijac.13164.
[29] V.H. Le, C. Nhan, H. Thuc, H.H. Thuc, Synthesis of silica nanoparticles from Vietnamese rice husk by sol-gel method, Nano scale Res. Lett. 8 (2013) 58.
[30] Y. Min, M. Akbulut, K. Kristiansen, Y. Golan, J. Israelachvili, The role of inter particle and external forces in nanoparticle assembly, Nat. Mater. 7 (2008) 527–538.
[31] https://www.sigmaaldrich.com/catalog/product/aldrich/420832?lang=en&region=IN&gclid=EAIaIQobChMI_MOt1-m14AIVRRSPCh2UwArBEAAYASAAEgK9HPD_BwE. (Accessed 12 February 2019).
[32] https://www.seair.co.in/colloidal-silica-import-data.aspx. (Accessed 12 February 2019).
[33] K. Liu, Q. Feng, Y. Yang, G. Zhang, L. Ou, Y. Lu, Preparation and characterization of amorphous silica nanowires from natural chrysotile, J. Non-Cryst. Solids 353 (2007) 1534–1539.
[34] Munasir, Z.A.I. Supardi, Mashadi, Z. Nisa, D.H. Kusumawati, N.P. Putri, A. Taufiq, Sunaryono, N. Hidayat, Darminto, Phase transition of SiO2 nano-particles prepared from natural sand: the calcination temperature effect, J. Phys. Conf. Ser. 1093 (2018), 012025, https://doi.org/10.1088/1742-6596/1093/1/012025.
[35] S. Lamouria, M. Hamidouche, N. Bouaouadja, Q.H. Belhoucheta, V. t Garnier, G. Fantozzi, J.F. Trelkat, Control of the γ-alumina to α-alumina phase transformation for an optimized alumina densification, Bol. Soc. Esp. Cerám. Vidr. (2016), https://doi.org/10.1016/j.bsecv.2016.10.001.
[36] K. Okada, J. Kaneda, Y. Kameshima, A. Yasumori, T. Takei, Crystallization kinetics of mullite from polymeric Al_2O_3–SiO_2xerogels, Mater. Lett. 57 (2003) 3155–3159.
[37] S. Bhattacharyya, R. Singh, Effect of solution pH on mullite phase formation from a diphasic precursor powder, J. Aust. Ceram. Soc. 52 (2) (2016) 20–31.
[38] D. Janackovi, V. Jokanovic, L.K. Gvozdenovic, L. Zivkovic, D. Uskokovic, Synthesis, morphology, and formation mechanism of mullite particles produced by ultrasonic spray pyrolysis, J. Mater. Res. 11 (7) (1996) 1706–1716.
[39] A.K. Singh, R. Sarkar, Nano mullite bonded refractory castable composition for high temperature applications, Ceram. Int. 42 (2016) 12937–12945.
[40] A.K. Singh, R. Sarkar, Development of spinel sol bonded high pure alumina castable composition, Ceram. Int. (2016), https://doi.org/10.1016/j.ceramint.2016.08.041i.
[41] S. Ghosh, R. Majumdar, B.K. Sinhamahapatra, R.N. Nandy, M. Mukherjee, S. Mukhopadhyay, Microstructures of refractory castables prepared with sol–gel additives, Ceram. Int. 29 (2003) 671–677.
[42] M.A.L. Braulio, G.G. Morbioli, J. Medeiros, J.B. Gallo, V.C. Pandolfelli, Nano-bonded wide temperature range designed refractory castables, J. Am. Ceram. Soc. 95 (3) (2012) 1100–1104.
[43] D.P.H. Hasselman, Unified theory of thermal shock fracture initiation and crack propagation in brittle ceramics, J. Am. Ceram. Soc. 52 (1969) 600–604.
[44] W. Qiu, G. Ruan, Z. Zhang, Properties of silica sol bonded corundum-spinel castables for steel ladles, Int. J. Appl. Ceram. Technol. 15 (2018) 1182–1189, https://doi.org/10.1111/ijac.12885.

Nomenclature

RH: Rice husk
RHA: Rice husk ash
BFS: Blast furnace slag
CAC: Calcium Aluminate cement
TEM: Transmission electron microscopy
XRD: X-ray diffraction
SEM: Scanning electron microscopy
DTA-TGA: Differential thermal & thermogravimetric analysis
BD: Bulk density
AP: Apparent porosity
CMoR: Cold modulus of rupture
CCS: Cold compressive strength
HMoR: Hot modulus of rupture
TSR: Thermal shock resistance
C: Corundum
M: Mullite
P: Pores
L:: Liquid

Please cite this article as: S.S. Hossain, P.K. Roy, Waste rice husk ash derived sol: A potential binder in high alumina refractory castables as a replacement of hydraulic binder, Journal of Alloys and Compounds, https://doi.org/10.1016/j.jallcom.2019.152806